Measurement of CP violation with the LHCb experiment

Judith Gnade
judith.gnade@tu-dortmund.de

Hendrik Lauersdorf
hendrik.lauersdorf@tu-dortmund.de

John Wendel
john.wendel@tu-dortmund.de

July 4, 2022

TU Dortmund – Fakultät Physik

Contents

1 Theoretical foundations

1.1 *CP* violation

CP violation describes a symmetry violation after applying charge conjugation C and parity conjugation P. Applying the C operator reverses the charge of a particle while applying the P operator is doing the same but with space components. While electromagnetic interactions are invariant after applying the *CP* operator, the strong and the weak interactions are not. *CP* violation in strong interactions is allowed in theory but not yet discovered. In weak interactions C and P are heavy violated but in most decays *CP* violation is neglible. *CP* violation can be found in several decays but are sizeable in B meson and kaon decays .
In the standard model quarks flavor eigenstates are not equal to their mass eigenstates. These eigenstates are connected by the CKM matrix. A complex phase in the CKM elements is responsible for the *CP* violation.
A *CP* violation means that either one, matter or anti matter, is preferred in some interactions. Since our universe contains much more matter than anti matter, some kind of *CP* violation has to exist. The known *CP* violation mechanisms are too small to explain such big discrepancies between matter and anti matter. That is why it is most likely that more, yet undetected, *CP* violating mechanisms exist. Searching for them might lead to the discovery of new physical processes or interactions.

1.2 Decay of *B* mesons

In this analysis the decays

$$B^{\pm} \to h^{\pm}h^{\pm}h^{\mp} \tag{1}$$

will be studied where $h^{\pm}$ are charged kaons or pions. The examined decays are described by the weak interaction as described earlier. A possible *CP* violation would be shown in a discrepancy between the number of B^+ and B^- mesons in a given dataset.
Since B mesons cannot be detected directly, they are reconstructed via the final state particles. It has to be taken into account that B mesons can decay through resonances involving charm quarks into the final state particles. In low orders the CKM matrix elements involving charm quarks do not have the complex phase responsible for *CP* violation. Therefore these resonances will be removed. The particles involved in this kind of decay are D mesons, J/ψ mesons and χ mesons.

2 The LHCb detector

The LHCb detector [2] is located at the Large Hadron Collider (LHC) at the nuclear research institute CERN. The detector is a foreward spectrometer specialized in measuring B mesons. It consists of different components which are briefly described here. The schematic structure of the detector components is also shown in figure 1.

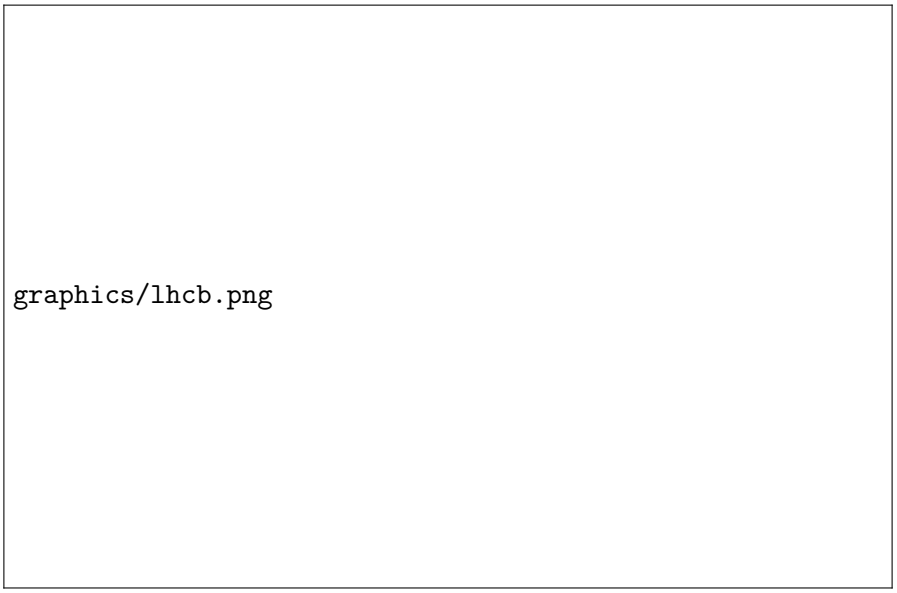

Figure 1: Components of the LHCb detector. [2]

The Vertex Locator (VELO) consists of several silicon modules and is constructed to measure the location of the proton-proton collision vertex as well as secondary B meson vertices. This is neccessary because due to the relatively long lifetime and therefore relatively large flight distances of B mesons. TT, T1, T2 and T3 are the silicon tracking detectors build to reconstruct particle tracks. T1-T3 also contain tube modules filled with a mixture of argon and carbondioxide. These gases are being ionized by particles resulting in a measurable signal. To get the particles' momenta, a magnet with an integrated magnetic field of 4 mT is used to measure the curvature of the charged partilce's tracks. This curvature determines the momentum of each charged particle. To lower systematic uncertainties, the polarity of this magnet is reversed frequently. The Cherenkov detectors RICH1 and RICH2 give information about the particle velocity using the cherenkov effect. RICH1 gives information about low momentum charged particles using aeorgel and C_4F_{10} radiators while RICH2 gives information about high momentum charged particles using a CF_4 radiator. Combining the information of momentum and velocity can determine the mass of a particle. The calorimetersystem consists of a scintillating pad (SPD), a preshower detector (PS), an electromagnetic calorimeter (ECAL) and a hadronic calorimeter (HCAL). Here most of the particles (with the exception of muons) deposit all their energy. The shower cluster of the deposited energy gives more information on which particle has been detected. Since muons are minimal ionizing particles, they cannot be stopped in the calorimeters. Therefore muon chambers are installed consisting of five stations (M1-M5).
To reduce the amount of data taken, a trigger system is used. The trigger system consists of a hardware component and a software component. The hardware component uses information from the calorimeters and muon chambers while the software component

reconstructs the event in real time and decides if the event is from interest.

3 Analysis Strategy

This analysis uses two data sets. One contains simulated events of the decay $B^{\pm} \to \mathrm{K}^{\pm}\mathrm{K}^{+}\mathrm{K}^{-}$ while the other are measurements from the LHCb experiment of the year 2011 with an integrated luminosity of $434\,\mathrm{pb}^{-1}$ for the up polarity of the magnet and $584\,\mathrm{pb}^{-1}$ for the down polarity. These measurements were selected on the same decay as the simulated data. After preselecting the data set by applying cuts in particle identification variables, global *CP* violation in this data set is investigated. By cutting on their respective masses, charmonium resonances are being removed by using a Dalitz plot. At the end studies on local *CP* violation are made by using the remaining data.

4 Analysis

4.1 Invariant mass of simulated B mesons

The mass of the B mesons cannot be determined directly. Therefore it is calculated via the final state particles in the given simulated data set. In the case of the decay

$$B^{\pm} \to \mathrm{K}^{\pm}\mathrm{K}^{+}\mathrm{K}^{-}\,.$$

the B mass is given by the mass and momenta of the three kaons with the relativistic relation of

$$\mathrm{E}^2 = \mathrm{p}^2 + \mathrm{m}^2\,. \tag{2}$$

The distribution of the three momentum components of one kaon is shown in figure 2. The x and y components have a very similar distribution due to symmetrical reasons since both are transversal components of the momentum. The z component of the kaon momentum has a different distrubution since it is the longitudinal component directing in the direction of the proton-proton beam. To calculate the magnitude of the momentum the relation

$$p = \sqrt{p_x^2 + p_y^2 + p_z^2} \tag{3}$$

is used. Together with the kaon mass of 493,677 MeV [3] the energy of the kaons is calculated using (2). The resulting energy distribution of the first kaon candidate is shown in figure 3. Because of conservation of energy the energy of the B meson is equal to the sum of the energies of the three kaons. The components of the momentum of the B meson are calculated like

$$p_i(B) = p_i(K_1) + p_i(K_2) + p_i(K_3), \tag{4}$$

where i can be x, y or z indicating the component of the momentum and K_1, K_2 and K_3 are the three kaons. To get the magnitude of momentum (3) is used again.
By using the relation (2), this leads to an invariant mass distribution of the B meson as shown in figure 4. The figure shows a sharp peak at the location of the known B mass of 5279,26 MeV [3].

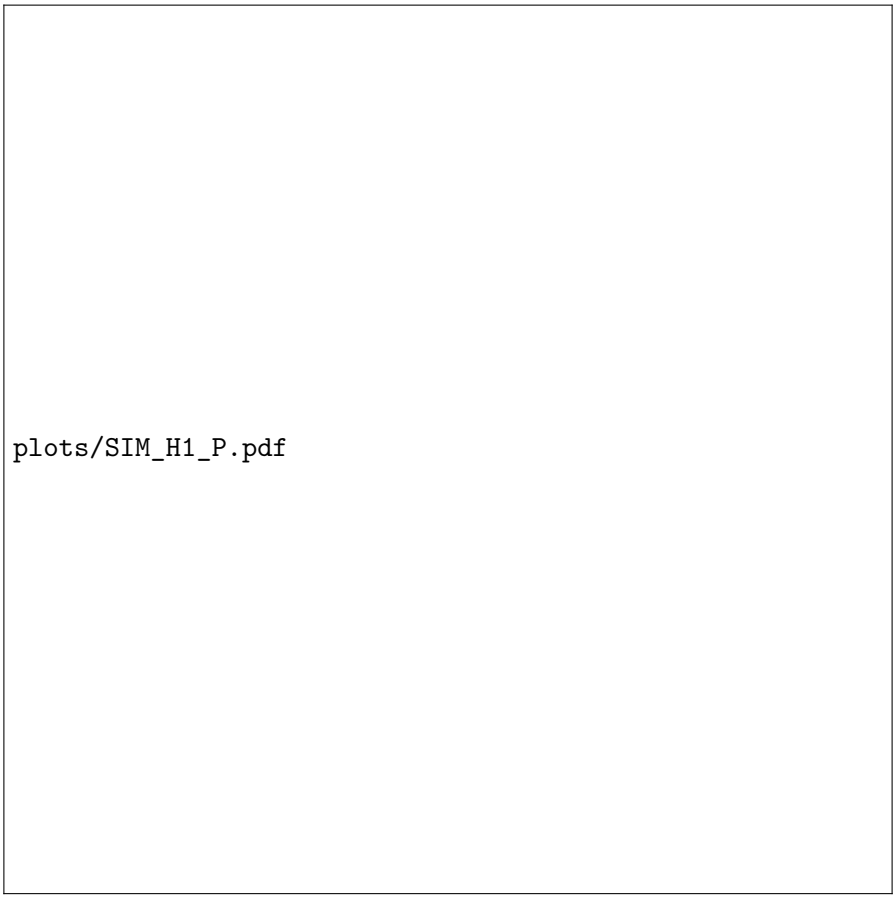

Figure 2: The three components x, y and z of the momentof of the first kaon candidate.

4.2 Invariant mass of measured B mesons

Before calculating the invariant mass of the measured B mesons, a preselection is applied. The following cuts are taken on the given data:

1. $\texttt{H}_n\texttt{\_isMuon} == \text{False}$
2. $\texttt{H}_n\texttt{\_ProbPi} < 0.5$
3. $\texttt{H}_n\texttt{\_ProbK} > 0.5$

In this case n can be 1, 2 or 3 indicating that the cuts are applied on all three final state hadrons. The boolean `isMuon` indicates if the identified particle is classified as a muon. `ProbPi` and `ProbK` show the probability of the hadron being a pion or a kaon. These variables are shown for the first hadron in figure 5a and 5b. The variables of the other hadrons possess a similar distribution.
The invariant mass of the B meson is calculated analog to the previous section. This leads to the distribution shown in figure 6. It shows some differences to the simulated

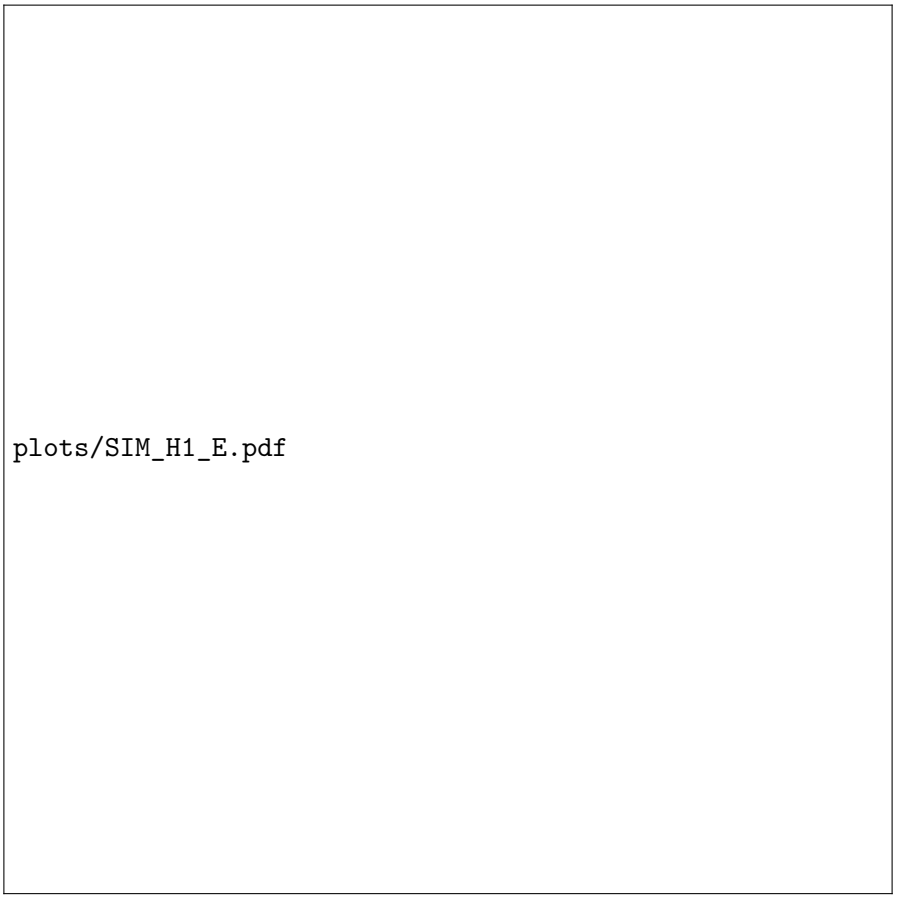

Figure 3: Energy distribution calculated from the mass and momentum of the first kaon candidate.

data set. On the lower and higher mass side there are some background events showing up. Beside that the mass peak is more smeared out due to energy fluctuations and resolution effects. Since changing the cuts on the ProbPi and ProbK variables seem to cut away a lot of events in the signal region while leaving most of the background events in the mass side bands, these variable cuts are not changed in any way. For the further analysis cuts on the B mass are being made since the mass side bands mostly contain combinatorial and partial reconstructed background. The following mass region will be analyzed in the following:

$$5200 < B\_M < 5350\,,$$

where `B_M` is the reconstructed mass in MeV. The remaining events are shown in figure 7.

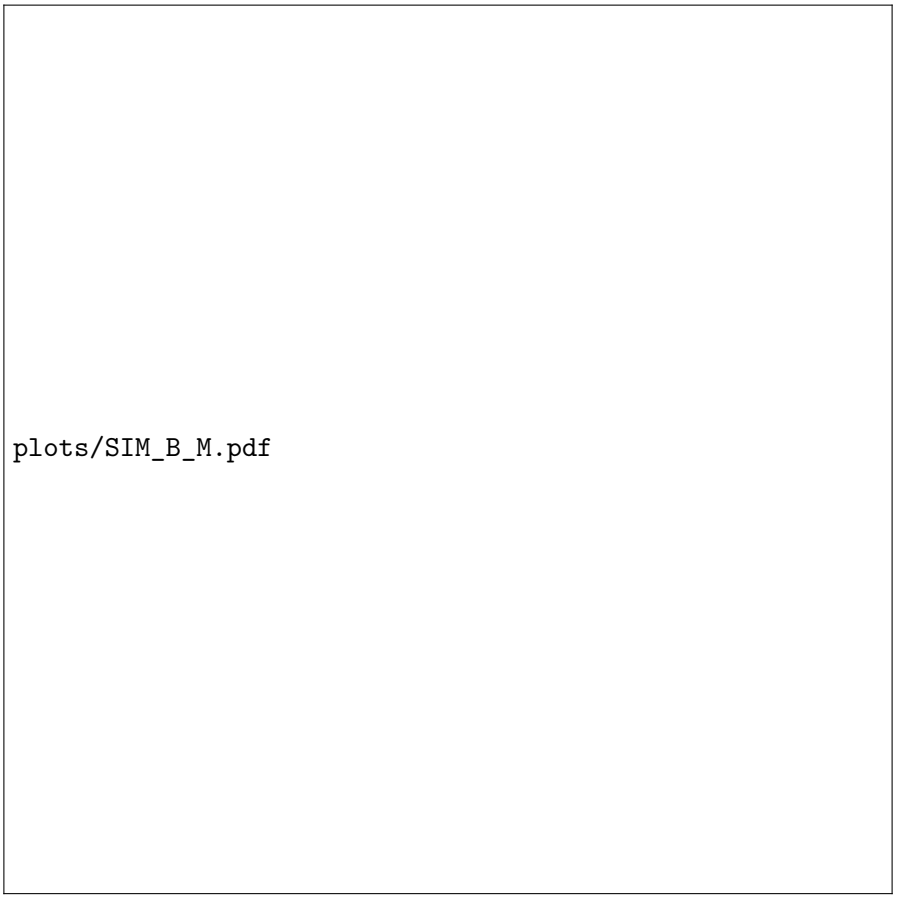

Figure 4: Invariant mass distribution of the simulated B mesons.

4.3 Search for global CP violation

To measure CP violation in general, the number of decays with B^+ (N^+) and with B^- (N^-) has to be known. To get the charge of a B meson, the charge of the final states kaons has to be taken into account:

$$Q(B) = Q(K_1) + Q(K_2) + Q(K_3) \tag{5}$$

where Q is the charge of the corresponding particle with a value of ± 1. After getting (N^+) and (N^-) by counting the remaining events, the global CP asymmetry is calculated by using

$$A = \frac{N^+ - N^-}{N^+ + N^-} = -0.0502. \tag{6}$$

(a) ProbPi with a cut at ProbPi < 0.5 **(b)** ProbK with a cut at ProbK > 0.5

Figure 5: ProbPi and ProbK for the first kaon candidate.

The corresponding statistical uncertainty and the statistical significance have values of

$$\sigma_A = \sqrt{\frac{1 - A^2}{N^+ + N^-}} \approx 0.0077 \tag{7}$$

$$\text{significance} = \frac{\mathrm{A}}{\sigma_A} \approx 6.5035\,. \tag{8}$$

The sicnificance of $6.5\,\sigma$ would usually mean a discovery of *CP* violation. However in this case no systematic uncertainies are being considered yet. By considering a production asymmetry of $1\,\%$ the corrected significance has just a value of $3.978\,\sigma$, having a value smaller that $5\,\sigma$ so it can only be considered as an evidence of *CP* violation.

4.4 Dalitz plots and two-body resonances

An important method used in three-body decays are Dalitz plots. The decay $B^\pm \to \mathrm{K}^\pm\mathrm{K}^+\mathrm{K}^-$ can be a direct decay or via $B^\pm \to \mathrm{K}^+\mathrm{R}^0$ where R^0 is an uncharged particle decaying into K^+K^-. Since the measured kaons are enumerated, there are three combinations of final state particles with two-body resonances:

1. $R_1^0 \to K_1^+ K_2^-$
2. $R_2^{++} \to K_1^+ K_3^+$
3. $R_3^0 \to K_3^+ K_2^-$

The double charged resonance R^{++} is not expected. The charge of a $q\bar{q}$ pair cannot be added to a value of 2. This leads to two remaining resonances: R_1^0 and R_3^0. These R^0 resonances can be shown in a Dalitz plot.

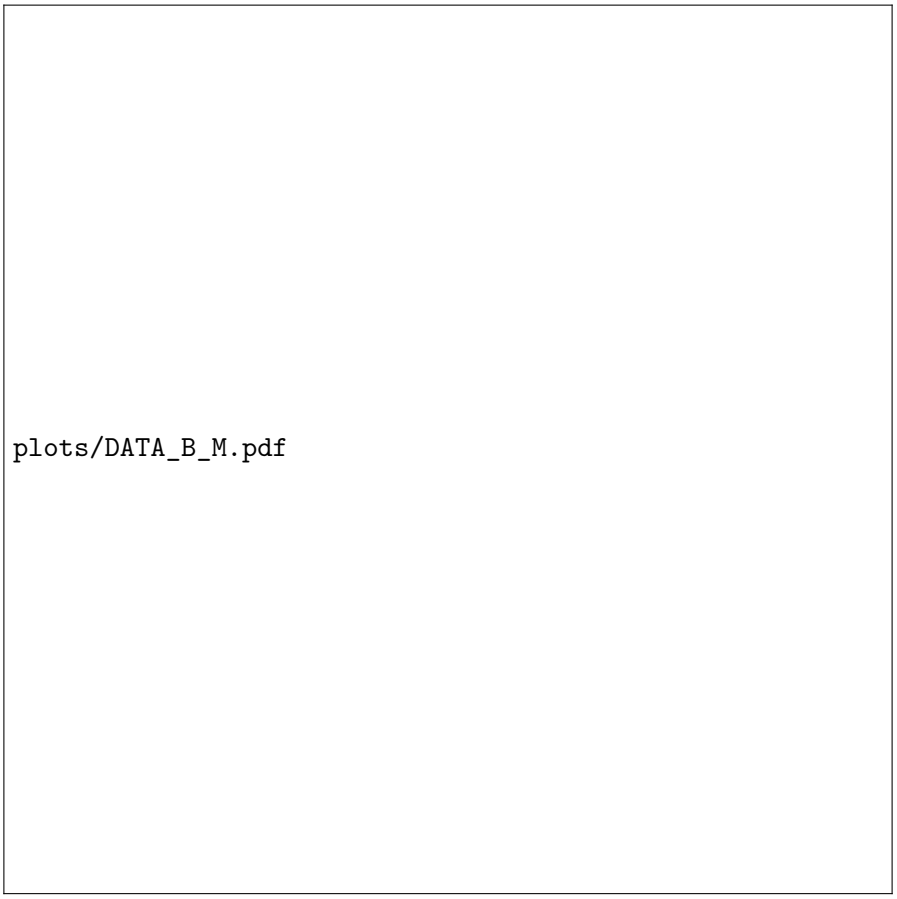

Figure 6: Invariant mass distribution of the measured B mesons.

The momenta and energies of the three final state kaons are not independent since these are conserved quantities. By plotting the invariant mass squares of just two of the three kaons, it is possible to identify resonances occuring in the data. Figure 8a shows a Dalitz plot for the simulated data. The plot shows an even distribution of the kinematicaly allowed region of energies and momenta. The Dalitz plot of the measured data is shown in figure 8b. Two resonance lines are recognizable. To highlight these lines even more the resonance masses are being sorted. The invariant masses m_{12} and m_{23} are being compared and the bigger mass is sorted into R^0_{max} and the lower mass into R^0_{min}. By using these as Dalitz variables the Dalitz plot now shows a more compromised kinetical area with more visible lines due to a higher event density.
This is shown in figure 9.
A binned version of the Dalitz plot is being produced to highlight the resonance lines in. The binned Dalitz plot is shown in figure 10 The first visible line with an invariant mass squared of approximately $1{,}2 \cdot 10^7\,\text{MeV}^2$ leads to a mass of $M \approx 3464\,\text{MeV}$. The particle closest to this mass is the $\chi_{c0}(1P)$ with a mass of 3414 MeV which is decaying into K^+K^- with a branching fraction of $(6.05 \pm 0.31) \times 10^{-3}$[3]. The reason for the

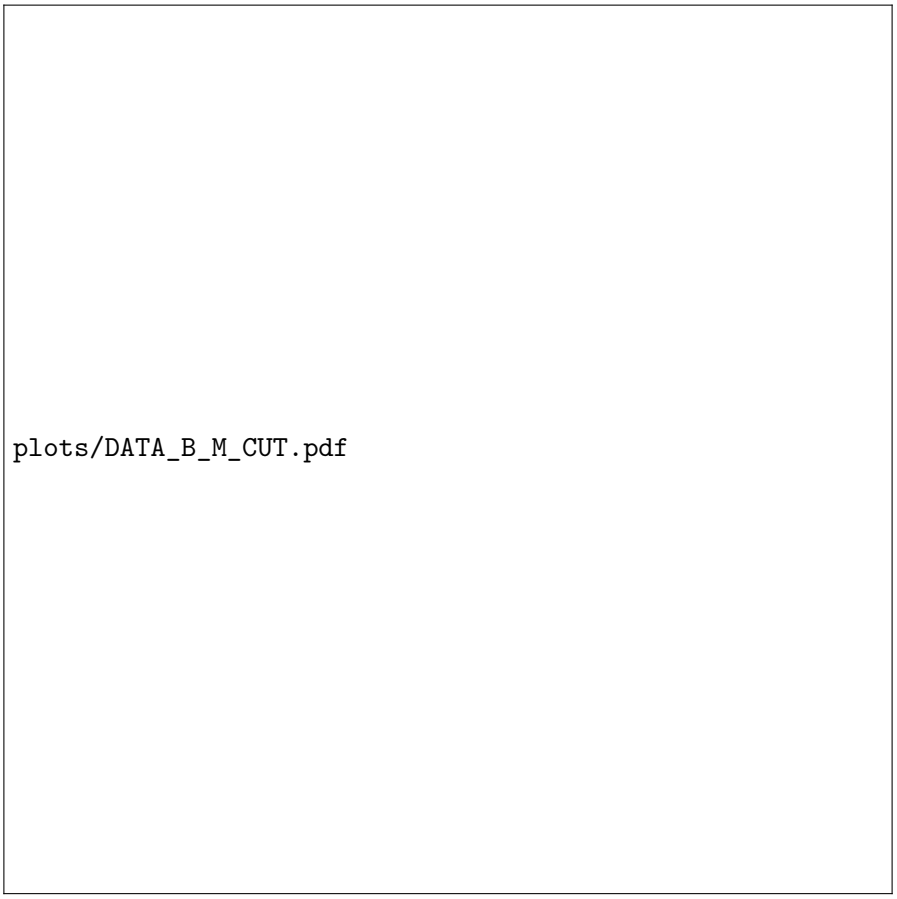

Figure 7: Invariant mass distribution of the measured B mesons with cuts on the B mass.

discrepancy of the $\chi_{c0}(1P)$ mass and the resonance line is that the position of the line is just estimated and the events in the line do not form a perfect line but a distribution. The second resonance is at an invariant mass squared of approximatelly $0{,}3 \cdot 10^7\,\mathrm{MeV}^2$. The corresponding resonance mass is $M \approx 1732\,\mathrm{MeV}$. The particle this mass belongs to is the D^0 with a mass of 1864 MeV decaying into K^+K^- with a branching fraction of $(4.08 \pm 0.06) \times 10^{-3}$[3]. Another particle which is in this mass region decaying into K^+K^- is the J/ψ with a mass of 3096 MeV. Even though the mass is not directly on the resonance lines of the Dalitz plots, it is still being taken into account. After cutting on the $\chi_{c0}(1P)$, D^0 and J/ψ masses with the cuts

$$\begin{aligned} 1800\,\mathrm{MeV} < B_M < 1900\,\mathrm{MeV} \\ 3080\,\mathrm{MeV} < B_M < 3120\,\mathrm{MeV} \\ 3380\,\mathrm{MeV} < B_M < 3450\,\mathrm{MeV} \end{aligned}$$

the two Dalitz plots from B^+ and B^- decays are being compared. These are shown in figure 11a and 11b.

(a) Dalitz plot of the simulated $B^{\pm} \to K^{\pm}K^{+}K^{-}$ data.

(b) Dalitz plot of the measured data containing resonances.

Figure 8: Dalitz plots of simulated and measured data.

Figure 9: Dalitz Plot with R^2_{max} and R^2_{min} as Dalitz variables.

Since both plots look very similar, an asymmetry plot with bigger binning is made as well as a plot to show the uncertainties and the significance. This also allows to calculate the binned asymmetries. These plots are shown in figure 12.

Figure 10: Binned Dalitz plot of measured data showing resonance lines.

(a) Binned Dalitz plot of B^+.

(b) Binned Dalitz plot of B^-.

Figure 11: Binned Dalitz plots of both $B^{\pm}$ decays after cutting out the resonances.

In figure 12c the region

$$0{,}6 \cdot 10^7\,\mathrm{MeV}^2 < R^2_{\mathrm{max}} < 1{,}3 \cdot 10^7\,\mathrm{MeV}^2$$
$$0{,}1 \cdot 10^7\,\mathrm{MeV}^2 < R^2_{\mathrm{min}} < 0{,}3 \cdot 10^7\,\mathrm{MeV}^2$$

shows the largest significance. The invariant mass distribution of B^+ and B^- decays in that region is shown in figure 13. It shows the difference in B^+ and B^- events indicating

(a) Binned Dalitz plot showing the asymetry of B^+ and B^-.

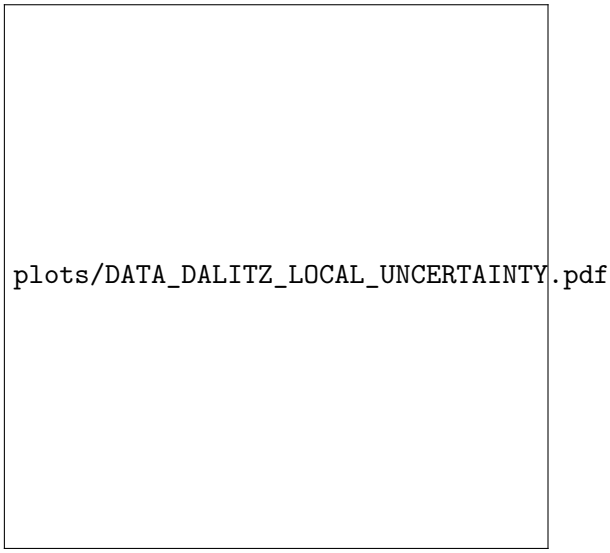

(b) Uncertainty of the asymetry.

(c) Significance of local *CP* violation

Figure 12: Asymmetry, uncertainty and significane comparing B^+ and B^- decays.

local *CP* violation.
After calculating the statistical uncertainty and significance, this leads to a value of

$$A_{\text{local}} = -0.154 \pm 0.017(\text{stat.})$$

This results in a significance of $8.99\,\sigma$. After taking the systematic uncertainty of $1\,\%$ into account caused by production asymmetry there is still a significance of $7.77\,\sigma$. This is an evidence of local *CP* violation in the decay $B^\pm \to \mathrm{K}^\pm\mathrm{K}^+\mathrm{K}^-$.

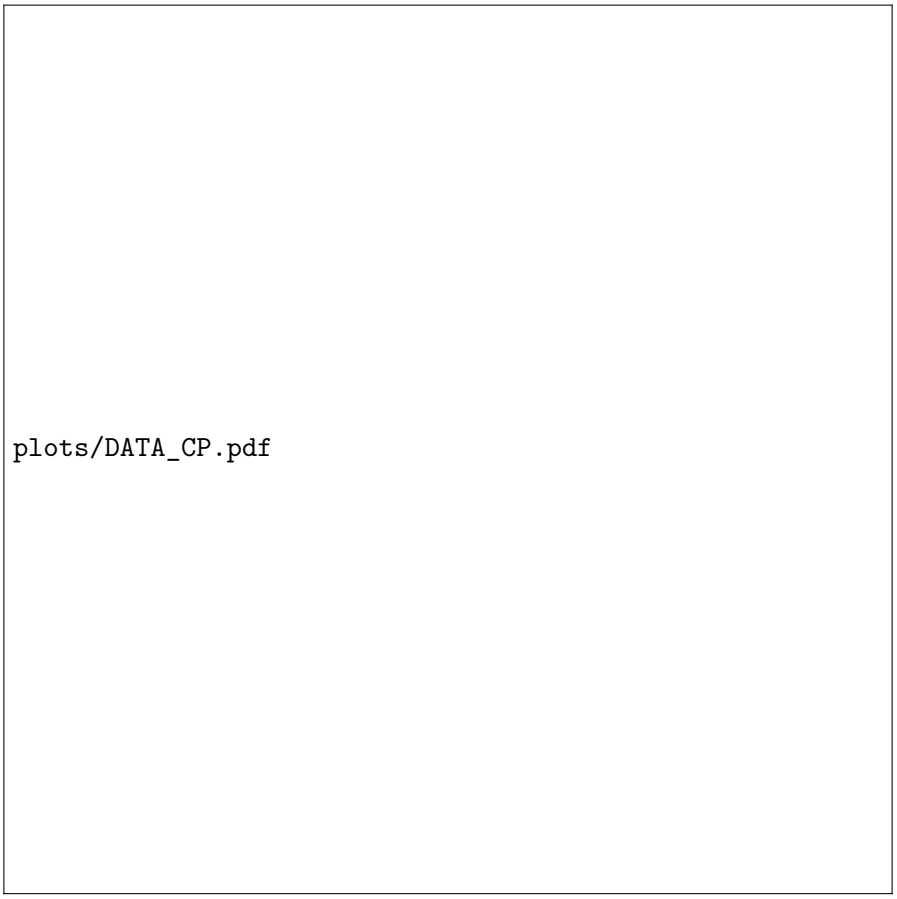

Figure 13: Comparison of B^+ and B^- events showing the local *CP* violation.

5 Discussion

Comparing simulated data with measured data shows a much sharper peak at the B mass in simulated data. This is because detector resolution effects were not simulated in this data set. These effects would smear out the distribution of events as seen in the measured data set. Connected to that is the position of the cut of the particle identification variables. It shows that harder cuts would cause a significant signal loss. In this analysis no special method was used to determine these cuts so a detailed analysis of this might cause more accuracy.
The global *CP* asymmetry shows a significance of nearly $4\,\sigma$. This is an evidence on global *CP* asymmetry but not an observation since the significance is smaller than $5\,\sigma$. In this analysis the only source of systematic uncertainties is production asymmetry. Including effects like detector effects and uncertainties in luminosity might give more accurate results. The LHCb paper [1] used the same data set and included systematic uncertainties in trigger asymmetrie and acceptance correction.
The Dalitz plots showed charmonium resonances in the data set. To make a more pure

set these resonances were cut out at their respective masses.
Local *CP* asymmetry shows a significance of $7.77\,\sigma$ yielding an observation of local *CP* asymmetry. This significance includes the statistical uncertainty and a 1 % uncertainty from production asymmetry. The location of this local *CP* asymmetry was delivered from the binned Dalitz plot. More analyses on binning and optimal location could lead to improvement of this results. To increase the accuracy the systematic uncertainies mentioned before should be taken into account as well.
Comparing the B^+ and B^- shows a clearly larger amount of B^- events.
In this analysis only the decay of a B meson into three kaons is studied since the background of this decay is the lowest. Decays with pions in the final state have larger backgrounds. Analyzing these decay channels might indicate more information on *CP* violation and give more statistics due to the higher branching ratio.

References

[1] R. Aaij et al. "Measurement of CP Violation in the Phase Space of $B^{\pm} \to K^{\pm}\pi^{+}\pi^{-}$ and $B^{\pm} \to K^{\pm}K^{+}K^{-}$ Decays." In: *Physical Review Letters* 111.10 (2013). ISSN: 1079-7114.

[2] The LHCb Collaboration et al. "The LHCb Detector at the LHC." In: *Journal of Instrumentation* 3.08 (2008).

[3] P.A. Zyla et al. "Review of Particle Physics." In: *PTEP* 2020.8 (2020).